Draft version July 15, 2010
Preprint typeset using LaTeX style emulateapj v. 11/10/09

MOMENTUM DRIVING: WHICH PHYSICAL PROCESSES DOMINATE AGN FEEDBACK?

Jeremiah P. Ostriker[1,2], Ena Choi[1], Luca Ciotti[3], Gregory S. Novak[1], and Daniel Proga[4]
[1]Department of Astrophysical Sciences, Princeton University, Princeton, NJ 08544, USA
[2]IoA, Cambridge, UK
[3]Department of Astronomy, University of Bologna, via Ranzani 1, I-40127, Bologna, Italy and
[4]Department of Physics and Astronomy, University of Nevada, Las Vegas, NV, USA

Draft version July 15, 2010

ABSTRACT

The deposition of mechanical feedback from a supermassive black hole (SMBH) in an active galactic nucleus (AGN) into the surrounding galaxy occurs via broad-line winds which must carry mass and radial momentum as well as energy. The effect can be summarized by the dimensionless parameter $\eta = \dot{M}_{\rm outf}/\dot{M}_{\rm acc} = 2\epsilon_{\rm w}c^2/v_{\rm w}^2$ where $\epsilon_{\rm w}$ ($\equiv \dot{E}_{\rm w}/(\dot{M}_{\rm acc}c^2)$) is the efficiency by which accreted matter is turned into wind energy in the disc surrounding the central SMBH. The outflowing mass and momentum are proportional to η, and many prior treatments have essentially assumed that $\eta = 0$. We perform one- and two-dimensional simulations and find that the growth of the central SMBH is very sensitive to the inclusion of the mass and momentum driving but is insensitive to the assumed mechanical efficiency. For example in representative calculations, the omission of momentum and mass feedback leads to an hundred fold increase in the mass of the SMBH to over $10^{10}M_{\odot}$. When allowance is made for momentum driving, the final SMBH mass is much lower and the wind efficiencies which lead to the most observationally acceptable results are relatively low with $\epsilon_{\rm w} \lesssim 10^{-4}$.

Subject headings: accretion, accretion discs – black hole physics – galaxies: active – galaxies: nuclei – galaxies: starburst – quasars: general

1. INTRODUCTION

Feedback from active galactic nuclei (AGNs) at the centers of galaxies is believed to have a significant effect on the evolution of those galaxies. However, the precise physical mechanisms by which this feedback occurs are greatly uncertain—perhaps more so than is commonly acknowledged. While much path-breaking and insightful work has been done, it is also true that some of the most basic requirements, such as the necessity that mass, energy, and momentum be conserved, have not been imposed in several of the popular treatments of this subject. And the inclusion of the presently known and observed feedback processes is often treated selectively. The purpose of this paper is to attempt to lay out the physical framework for discussing the issues and to provide illustrative examples of the results obtained primarily from one-dimensional computations that include or exclude specific processes. We also include a treatment of the two-dimensional, axisymmetric case, presented in less detail, to show how the qualitative features carry over to this more realistic case. Definitive solutions are beyond present art in this field, so the focus will be on the qualitative features of the physical solutions rather than the detailed comparison with observations.

In outline, there are three phases to the overall phenomenon: 1) the provision of fuel for the central supermassive black hole (hereafter SMBH); 2) the generation of the outflowing stream of energy, mass and momentum from the vicinity of the SMBH; and 3) the absorption and transmission of this energy, mass and momentum by the ambient gas in the galaxy and the subsequent reactions of the ambient gas to that input.

1. The fueling is generally believed to be via infalling gas, and typically, two origins for that gas have been proposed; at high redshift ambient gas in discs liberated by the non-axisymmetric forces released during mergers is certainly important (Barnes & Hernquist 1991), while at lower redshift mergers fail and probably do not fuel AGNs (Li et al. 2001), but the processed gas released via normal stellar evolution provides an ample source (Mathews 1983; Shull 1983; Ciotti et al. 1991; Padovani & Matteucci 1993; Ciotti & Ostriker 2007, hereafter CO07). A primary clue as to which of these sources dominates in a specific case is provided by details of the metallicity distribution, since the reprocessed gas probably has super-solar metal abundance and will also show signs of stellar evolution such as higher nitrogen or S-process abundances. The clue to fueling by infalling globular clusters might be relatively low abundances of elements made in SN I such as Fe. In almost all treatments a central disc mediates between the inflowing material and the SMBH. Other sources, such as small stellar systems dragged in by dynamical friction have been considered from time to time. These stars, or others added to the central regions via loss-cone processes (Begelman, Blandford & Rees 1980) can be shredded during tidal interactions with the central SMBH or by collisions with one another or with a central disc—the debris collecting in the disc and feeding the central SMBH via conventional mechanisms (Ostriker 1983; Dai, Fuerst & Blandford 2010).

2. The outflows fall into three categories. The signature of AGNs is, of course, the enormous electromagnetic, luminous output, with major contributions from the IR bands to the gamma ray region. The bulk of the flux is typically in the "UV bump" and the flux from this region thus dominates for the "momentum driven winds" (e.g., see Proga, Stone & Kallman 2000; King 2003; Proga & Kallman 2004; DeBuhr et al. 2009). The region where this driving occurs is fairly

close to the quasar ($50R_{\rm BH} \lesssim r \lesssim 500R_{\rm BH}$, where $R_{\rm BH}$ is the SMBH Schwarzschild radius). However, the moderately hard X-rays determine the average photon energy: $\langle h\nu\rangle = h\int L_\nu \nu {\rm d}\nu / \int L_\nu {\rm d}\nu$ when integrated over the spectrum. This region of the spectrum dominates the photon heating, causing the heated gas to approach the mean photon energy: $1.5kT_X = \langle h\nu\rangle$ with $T_X \sim 2\times 10^7$K (Sazonov, Ostriker & Sunyaev 2004). The resultant heating occurs over an extended range of radii: 100 pc$< r <$3 kpc (Ciotti, Ostriker & Proga 2009, 2010, hereafter Papers I and III), and it can be significant for $r \gtrsim 0.1$ pc (Proga 2007). It can efficiently drive outflows as shown in a series of papers by Ciotti, Ostriker and collaborators (cf.CO07 and references therein). For electromagnetic output there is, of course, no rest-mass component. The total energy emitted in this form has been established fairly accurately via the Soltan (1982) argument to be $\Delta E = \epsilon_{\rm rad}\Delta M_{\rm acc}c^2$ with $\epsilon_{\rm rad}\sim 0.1-0.15$ (Yu & Tremaine 2002). The momentum output, of course, is $\Delta p = \Delta E/c$. In optically thick cases ($\tau \gg 1$), the total momentum absorbed by the fluid can approach $\Delta p = \tau \Delta E/c$ (DeBuhr et al. 2009). Silk & Nusser (2010) also consider the importance of radiative momentum driven winds on galactic and cluster scales but limit the input to L/c, which can be considerably less than allowed in the optically thick case by Ciotti & Ostriker (2007) or DeBuhr et al. (2009).

Next, let us turn to mechanical output. Both broad- and narrow-line regions inject mass, energy and momentum into the surrounding gas, with the broad-line winds probably dominant. Since these are material flows with velocity in the vicinity of the SMBH, $v_{\rm w}$, the mass outflow can be considerable. If we let the inflowing and outflowing mass rates be ($\dot M_{\rm inf}$, $\dot M_{\rm outf}$), then conservation of mass, energy and momentum can be summed up with the following simple equations:

$$\dot M_{\rm acc} = \dot M_{\rm inf} - \dot M_{\rm outf}, \tag{1}$$

where $\dot M_{\rm acc}$ is the mass rate actually accreted by the SMBH, and

$$\dot E_{\rm w} = \frac{1}{2}\dot M_{\rm outf} v_{\rm w}^2 \tag{2a}$$

$$= \epsilon_{\rm w}\dot M_{\rm acc}c^2, \tag{2b}$$

$$\dot p_{\rm w} = \dot M_{\rm outf} v_{\rm w}, \tag{3}$$

are the wind energy and momentum, respectively. We have oversimplified matters by allowing only one wind velocity, when in fact Equation 2a requires $\langle v_{\rm w}^2\rangle$ and Equation 3 requires $\langle v_{\rm w}\rangle$. Also, it is important to specify exactly where and when the quantities in equations 1–3 are to be measured. In the conventional treatment of this subject, the SMBH is surrounded by a disc or torus to which matter has fallen from larger radius. Then, placing a sphere around this disc or torus (at $r\sim 1$ pc), the instantaneous spherically averaged infall through the sphere is $\dot M_{\rm inf}(t)$ and the spherically averaged outflow is $\dot M_{\rm outf}(t)$. The difference will be accreted onto the SMBH unless driven out in disc originating winds; the latter of course contributes to $\dot M_{\rm outf}$ and so the remainder $\dot M_{\rm inf} - \dot M_{\rm outf}$ will be accreted. Two further complications are allowed for in some detailed treatments: (i) the actual instantaneous value of $\dot M_{\rm acc}$ is a time-lagged convolution of the quantity in Equation 1 since a finite time elapses as material is transported through the disc to the central SMBH and (ii) star formation may (in fact frequently will) occur in the disc, removing mass that would otherwise have accreted onto the SMBH. Both of these complications are allowed for in CO07 and other work, neither is of dominant importance.

Now, defining the dimensionless ratio from Equation 2a and 2b to be,

$$\eta \equiv \frac{\dot M_{\rm outf}}{\dot M_{\rm acc}} = \frac{2\epsilon_{\rm w}c^2}{v_{\rm w}^2}, \tag{4}$$

we can now rewrite Equations 1–3 as

$$\dot M_{\rm acc} = \dot M_{\rm inf}\frac{1}{1+\eta}, \tag{5a}$$

$$\dot M_{\rm outf} = \dot M_{\rm inf}\frac{\eta}{1+\eta}, \tag{5b}$$

$$\dot E_{\rm w} = \frac{1}{2}\dot M_{\rm inf} v_{\rm w}^2\frac{\eta}{1+\eta} = \epsilon_{\rm w}\dot M_{\rm inf}c^2\frac{1}{1+\eta}, \tag{5c}$$

$$\dot p_{\rm w} = \dot M_{\rm inf} v_{\rm w}\frac{\eta}{1+\eta}. \tag{5d}$$

These Equations, 5a-d, are, in fact, the ones that most authors have adopted who treat AGN feedback as a unified process comprising both infall and outflow. However, they typically adopt $\eta = 0$, implicitly assuming $v_{\rm w}\to\infty$, so that $\dot M_{\rm outf}$ and $\dot p_{\rm w}$ are neglected and the two terms that are included, $\dot E_{\rm w}$ and $\dot M_{\rm acc}$, may be overestimated. If it eventuated that η really is a very small number, then not much error would be induced and one would be justified in neglecting the out-flowing mass and momentum and in setting $\dot E_{\rm w}\sim\epsilon_{\rm w}\dot M_{\rm inf}c^2$, as most authors assume. If we adopt for the efficiency of generating mechanical energy the value $\epsilon_{\rm w} = 5\times 10^{-3}$, as done by Springel, Di Matteo, & Hernquist (2005); Johansson, Naab & Burkert (2009), hereafter SDMH05 and JNB09 respectively, McCarthy et al. (2010) and other authors, and we take $v_{\rm w} = 10^4$ km/s ($v_{\rm w,10}$) (Moe et al. 2009), then we have from Equation 4, $\eta = 9v_{\rm w,10}^{-2}$ and all of the neglected effects may in fact be dominant; the bulk of the inflowing mass may be ejected in a broad-line disc wind, and the mass and momentum input deposited in the ambient gas may dominate over the energy input, which may be largely radiated away. Papers I and Paper III do include these effects, but do not spell out their significance. The principal purpose of the present paper is to do just that—to show, in specially simple one- and two-dimensional calculations the effects of including or excluding mass, energy and momentum conservation when $\eta > 0$. In addition to the papers referred to above which attempt to compute both the infall to the central SMBH and the outflow from it in a unified fashion, there are many others which postulate a central source and then, after estimating the mass, momentum and energy flowing at of that source (and some angular and temporal distribution thereof) do effectively compute the effects of that injection of energy, mass and momentum onto the surrounding fluid. Space does not permit a comprehensive description of this related subject of research, but impor-

tant papers include the following: cf. Metzler & Evrard (1994); Sternberg & Soker (2008); Fabian et al. (2009); Reeves et al. (2009); Arieli, Rephaeli & Norman (2010); Gaspari et al. (2010).

The wind efficiency, $\epsilon_{\rm w}$, is not known very well—neither from observations nor from detailed physical simulations. But the best estimates from either of these sources might be in the range $1 \times 10^{-3} > \epsilon_{\rm w} > 3 \times 10^{-4}$ (Proga, Stone & Kallman 2000; Proga & Kallman 2004; Krongold et al. 2007; Stoll et al. 2009; Kurosawa, Proga & Nagamine 2009), a factor of 5 to 17 smaller than the commonly adopted values and in a range where $\eta \lesssim 1$ if $v_{\rm w,10} \approx 1$. A specific example may be useful. Moe et al. (2009) study the quasar SDSS J0838+2955. They find a mechanical energy output of 4.5×10^{45} erg/s, a mass outflow rate 10 times the accretion rate and a mechanical efficiency of 1×10^{-3}, and they quote other observational studies which indicate similar numbers. From analyses of the ionization parameters in the broad-line winds, estimates of the radial extent of the winds can be made; the above paper, and those quoted within indicate radii measured in kpc—consistent with the one-dimensional numerical work in Paper III.

As shown in Papers I and III, an additional important question asks "what fraction of the sky is covered with the broad-line winds?" Again two approaches are possible. Empirically, on the order of 20-25% of bright quasars show broad-line winds; this translates to $\sim \pi$ steradians or $\pi/2$ steradians in each conical outflow, if we assume that the wind is emitted symmetrically above and below the inner AGN disc. On the theory side, the radiation driven winds found by Proga & Kallman (2004), via detailed hydro radiation-transfer calculations, cover $\sim \pi$ steradians, roughly consistent with the observational estimates.

Finally, let us turn to the narrow jets, the outflow observed from AGN in "radio mode", when the electromagnetic luminosity is considerably below the Eddington limit. M87 is an excellent nearby example of such a system. These are standard FRI radio sources. Here the jets are quite narrow and appear to be comprised primarily of a relativistic fluid. The same type of calculation as presented in the last section would indicate that the out-flowing mass is of negligible importance and the energy output greatly dominates over the momentum output. The total energy output from these phases is considerable, but the accretion rates are thought to be low in these phases so the efficiencies of energy generation may be very high (cf. for a computation McKinney & Gammie 2004). Since so little mass is accreted in radio mode, the Soltan argument cannot be used to empirically estimate efficiencies, but, from the observational estimates of the energies available in the giant radio lobes, it may be that the AGN emits in radio mode considerably more energy than it does in wind mode. However the deposition from the intense but extremely narrow streams appears to be inefficient, and the jet drills through the gas in the surrounding galaxy, dumping most the energy into the intergalactic medium. Thus, while it may act as the dominant feedback mechanism for the IGM (and we will return to this in a subsequent paper), it is of lesser importance than the radiative or wind components in heating and driving out the ambient gas from within a galaxy.

3. The interactions between the out-flowing energy, mass and momentum with the ambient fluids are complex and are just beginning to be studied with the needed detail. We focus here on the relatively gas poor elliptical systems, since it is in these that the bulk of the mass in SMBHs is found, The radiative interactions are perhaps easiest to describe. Since the mechanical momentum is conserved and cannot be radiated away, it can be a dominant effect. The minimum level of interaction is provided by electron scattering and, since the most luminous quasars are found to be clustered near the Eddington luminosity limit (at which level the momentum absorbed by electron scattering balances the gravitational force on the fluid from the central SMBH), we know that this effect is significant in many cases. Absorption of the out-flowing radiation will not, in general, reduce this effect, since typically the radiation is simply re-emitted in another band and electron scattering opacity is wavelength independent until the Klein-Nishina limit is reached at very high energies. In fact, in the optically thick limit, the radiation is transformed by dust absorption into the infra-red, but the effects in this case are even greater than in the simple case, since the scattering opacity of the dust to infra-red is, per atom, larger (by roughly a factor of 5) than the electron scattering cross section. For the bright ULIRGs, which may contain both an active AGN and a brighter starburst, there will be a near balance between the inward gravitational forces and the outward radiative momentum transfer on the dust (cf. Thompson, Quataert & Murray 2005, CO07). Under these circumstances, the inner several hundred parsecs of the galaxy are analogous in their equilibrium structure to a very massive star in so far as there is a nearly equilibrium balance between radiative and gravitational forces.

The effects of heating from the AGN are, for quite different reasons, also likely to be independent of absorption (so long as it is not excessive, i.e. not Compton thick). Sazonov et al. (2005) present a simple analytical exploration of the effects and Paper I presents a more detailed one-dimensional treatment. The photons which dominate the heating process are in the moderately hard region ($\sim$50keV), and we know from X-ray absorption studies that AGN are typically optically thin to such radiation. Metal line resonance absorptions dominate the absorption unless the spectrum is extremely hard, and in those cases Compton absorption would be dominant. If we consider the issue on a per atom basis, all that matters is the heating per atom, which scales as r^{-2} (assuming that the fluid is optically thin to hard X-rays), and the cooling rate per atom which scales as the density. Since the latter can also scale as r^{-2} or even falls off at a steeper rate in some circumstances, the heating can balance or exceed cooling over an extended range of radii. If that happens, the gas temperature will rise towards the radiation temperature, $T_X \sim 2 \times 10^7$ K. Then, since this exceeds the virial temperature in almost all galaxies, the heated gas, having thermal energy higher than its gravitational energy, will be accelerated outwards and tend to drive a wind into the surrounding fluid. Of course, since this will shut off the accretion flow and the fuel to the central source, the result will be a burst of energy output followed by much slower cooling of the shocked gas and

a repeated burst at a much later time. Thus, episodic accretion is expected.

The mechanical energy input is more localized to the vicinity of the SMBH and would be efficient in "protecting" the SMBH from very high rates of accretion, except for one important caveat. It necessarily happens that such episodes of high rates of energy deposition will occur when the central gas densities are high, and under such circumstances the gas will tend to radiate away the input energy unless forbidden to do so as has occurred in some calculations (Booth & Schaye 2009). This, as we shall see, makes the energy input rather inefficient in driving outflows and in protecting the SMBH from excessive accreation. But the momentum input cannot be radiated away, and, as we shall see in the remainder of the paper, it is very efficient in limiting the infall and accretion onto the central SMBH. Mechanical input, via either thermal or momentum based mechanisms, will also tend to produces episodic accretion.

The broad-line gas outflow must drive a strong shock into the ambient gas, and that, in turn, given standard physics, should accelerate charged particles efficiently via a variant of the first order Fermi process (cf. Blandford & Ostriker 1978; Bell 1978; Blandford & Eichler 1987). Then this relativistic fluid will further drive the outflow and, since thermal radiation is suppressed for this component, the conversion may somewhat enhance the effects of feedback. But, overall, this process simply transforms internal energy from one form to another and so, whereas it may be observationally quite significant, it will have a relatively small global effect. Two recent papers that have explored these processes are Fujita et al. (2007) and Jiang et al. (2010); see also Sironi & Socrates (2010).

2. THE MODELS

In this section, we summarize the main properties of the galactic models adopted in this study. A detailed description of the galaxy models and input physics is given in CO07, Papers I and III.

We study galaxy models characterized by the effective radius of the galaxy stellar component $R_{\rm e} = 6.91$ kpc, an initial stellar mass $M_* = 2.87 \times 10^{11} M_\odot$, and central aperture velocity dispersion $\sigma_{\rm a} = 260$ km s^{-1}. This represents approximately the typical L_* galaxy which Yu & Tremaine (2002) find contain the bulk of the identified mass in SMBHs. The stellar mass distribution which is embedded in a dark matter halo is described by the Jaffe (1983) model while the total mass density distribution follows a r^{-2} profile; all the relevant dynamical quantities need in the simulation are given in Ciotti, Morganti & de Zeeuw (2009). The initial SMBH mass is $M_{\rm BH} = 2.87 \times 10^8 M_\odot$, following the Magorrian et al. (1998) relations ($M_{\rm BH} \sim 10^{-3} M_*$). The simulations are for an isolated, giant elliptical galaxy without the effect of the intracluster medium, as outflow boundary conditions are set at the galaxy outskirts ($\sim$ 250 kpc), so that the interstellar medium (ISM) is provided by the recycled gas produced by stellar evolution. The simulations starts at 2 Gyr, which corresponds to a redshift of $z \sim 3.2$ for the ΛCDM cosmology with $\Omega_m = 0.3$, $\Omega_\Lambda = 1 - \Omega_m = 0.7$ and $H_0 = 70$ km s^{-1} Mpc^{-1} and ends at 14 Gyr.

The input physics of the model is fully described in Paper I. Here we recall the most important aspects. The instantaneous bolometric accretion luminosity is

$$L_{\rm BH} = \epsilon_{\rm EM} \dot{M}_{\rm acc} c^2, \tag{6}$$

and we adopt an advection-dominated accretion flow (ADAF)-like radiative efficiency as

$$\epsilon_{\rm EM} = \epsilon_0 \frac{A\dot{m}}{1 + A\dot{m}}, \qquad \dot{m} \equiv \frac{\dot{M}_{\rm acc}}{\dot{M}_{\rm Edd}}, \tag{7}$$

where $\dot{M}_{\rm Edd} = L_{\rm Edd}/\epsilon_0 c^2$, and A is a free parameter so that $\epsilon_{\rm EM} \sim \epsilon_0 A\dot{m}$ for $\dot{m} \ll A^{-1}$. We fix $A = 100$ in our simulations (Narayan & Yi 1994), and we adopt for the peak EM efficiency $\epsilon_0 = 0.1$ or 0.2 consistent with estimates based on the Soltan (1982) argument. In the treatment of radiation feedback, we consider the radiation pressure as well as heating/cooling feedback, including photoionization, Compton and line heating (Sazonov, Ostriker & Sunyaev 2004; Sazonov et al. 2005). In accordance with both observations and theoretical expectation, the transformation of accreted mass to electromagnetic energy output declines dramatically at low accretion rates.

In the mechanical feedback treatment, the fiducial instantaneous mechanical luminosity of the disk wind is calculated as

$$L_{\rm dw} = \epsilon_{\rm w} \dot{M}_{\rm acc} c^2 + \epsilon_{\rm II} c^2 (1 - f_{\rm rem,h}) \frac{M_{\rm dh*}}{\tau_{*\rm h}} \tag{8}$$

where $\epsilon_{\rm w}$ is the mechanical efficiency of the wind, and the second term represents the energy associated with the Type II supernova (SNII) explosions of the high-mass stars in the circumnuclear disk (see Paper I, Equation (20) for details). Here, $M_{\rm dh*}$ is the current mass in the disc in high mass ($M > 8 M_\odot$) and $\tau_{*\rm h}$ is their typical lifetime. In this work, we restrict attention to the commonly assumed case of a constant value of $\epsilon_{\rm w}$ (e.g. SDMH05), which corresponds to Type A models in Papers I and III. Physically, a fixed mechanical efficiency implies that the mass accreted by the central SMBH has a fixed relation to the mechanical energy flowing out of the central regions. We here neglect the jet effects, which are expected to be effective only in the low-luminosity, hot accretion phases at late-time evolution. The reference models (A0 and A1) from Paper III study the evolution of gas and the mechanical feedback from SMBHs, and solve Eulerian equations of hydrodynamics with mass, energy, and momentum sources (see Paper I). In order to study the effect of each physical process, i.e., mass, energy, and momentum feedback, we build several models which neglect one or two of physical terms. We discuss the details of each model and comparison of them in the following section.

3. EXPLORING ONE-DIMENSIONAL MODELS

The model properties and results are given in Table 1. The mechanical efficiencies $\epsilon_{\rm w}$ are given in Column 3 and the corresponding values of $\eta \equiv 2\epsilon_{\rm w} c^2/v_{\rm w}^2$ are given in Column 4. We devote Column 5-9 to present ($z = 0$) model properties. First, for some models indicated with the symbol $\surd$ in Column 5, we distribute the mechanical feedback energy (momentum and mass) only at the lower boundary of the grids to

TABLE 1
Summary of One-dimensional Model Properties

				Bottom	Feedback							
	Model	$\epsilon_{\rm w}$	$\eta(v_{\rm w,10}^{-2})^a$	Layer^b	Radiation	Energy	Momentum	Mass	log $\Delta M_{\rm BH}$	log L_X	log $l_{\rm BH}^{\rm eff\ c}$	log $\Delta E_{\rm w}{}^d$
(1)	(2)	(3)	(4)	(5)	(6)	(7)	(8)	(9)	(10)	(11)	(12)	
1	A0 ^{e}	5×10^{-3}	9	×	√	√	√	√	6.72	37.11	-7.98	58.67
2	MA0 ^{e}	5×10^{-3}	9	×	×	√	√	√	6.72	37.11	-7.98	58.67
3	**EPM0-R**	$\mathbf{5\times10^{-3}}$	**9**	√	√	√	√	√	**7.07**	**39.75**	**-10.58**	**59.02**
4	EPM0	5×10^{-3}	9	√	×	√	√	√	7.13	37.84	-10.58	59.08
5	PM0	5×10^{-3}	9	√	×	×	√	√	7.13	37.84	-10.58	59.08
6	**E0** ^{f}	$\mathbf{5\times10^{-3}}$	**9**	√	×	√	×	×	**10.32**	**41.31**	**-3.61**	**62.27**
7	A1 ^{e}	2.5×10^{-4}	0.45	×	√	√	√	√	7.38	36.36	-6.72	58.02
8	MA1 ^{e}	2.5×10^{-4}	0.45	×	×	√	√	√	7.52	38.09	-6.48	58.17
9	**EPM1-R**	$\mathbf{2.5\times10^{-4}}$	**0.45**	√	√	√	√	√	**8.04**	**39.59**	**-8.23**	**58.69**
10	EPM1	2.5×10^{-4}	0.45	√	×	√	√	√	7.76	38.82	-8.15	58.41
11	PM1	2.5×10^{-4}	0.45	√	×	×	√	√	7.76	38.82	-8.15	58.41
12	**E1** ^{f}	$\mathbf{2.5\times10^{-4}}$	**0.45**	√	×	√	×	×	**10.33**	**41.29**	**-3.62**	**60.98**
13	EPM2-R	1×10^{-3}	1.8	√	√	√	√	√	7.59	40.13	-9.25	58.85
14	EPM3-R	1×10^{-4}	0.18	√	√	√	√	√	8.24	40.39	-7.79	58.50
15	EPM4-R	5×10^{-5}	0.09	√	√	√	√	√	8.29	40.03	-7.51	58.25
16	EPM5-R	2.5×10^{-5}	0.045	√	√	√	√	√	8.78	40.33	-5.77	58.43
17	EPM6-R	1×10^{-5}	0.018	√	√	√	√	√	9.11	40.50	-5.30	58.37
18	EPM7-R	5×10^{-6}	0.009	√	√	√	√	√	9.29	39.97	-5.14	58.24

Note. Model names (except for Model 1, 2, 7 and 8) indicate the activated physics (symbol √) in the simulations as detailed in Column 6-9. For example, in E0 and E1 models only mechanical energy feedback is allowed, while in PM0 and PM1 models momentum and mass are considered, but not mechanical energy. We adopt 0.2 for the peak EM efficiency ϵ_0.

[a] $\eta = 2\epsilon_{\rm w}c^2/v_{\rm w}^2$ in $v_{\rm w,10}^{-2}$ unit where $v_{\rm w} = 10,000$km/s

[b] Models with mass, energy and momentum added to the bottom layer.

[c] $l_{\rm BH}^{\rm eff} \equiv L_{\rm BH,opt}^{\rm eff}/L_{\rm Edd}$ where $L_{\rm BH}$ is the SMBH luminosity in the optical band after absorption, i.e., as it will be seen from infinity.

[d] $\Delta E_{\rm w} \equiv \epsilon_{\rm w}\Delta M_{\rm BH}c^2$, in erg, where $\Delta M_{\rm BH}$ is in $M_\odot$ units.

[e] These models correspond to the models A0, MA0, A1 and MA1 in Papers I and III, but calculated with some difference in the numerical grid spacing.

[f] The model similar to one adopted in SDMH05.

mimic the common treatment of mechanical feedback (e.g. SDMH05, Di Matteo, Springel & Hernquist 2005, JNB09). Instead, models indicated with the symbol × in Column 5 have a distributed feedback as in Papers I and III where we attempt to estimate the gradual deposition of mass, energy and momentum taken from the outflowing wind and going into the ambient gas as a function of radius. We then build several models which neglect one or two of physical process, i.e., mass, energy, and momentum feedback in order to study their effects showing the inclusion of each term in Column 6-9. For example, Model 3 (EPM0-R, in bold face) distributes the mechanical feedback only into the bottom layer, and includes the radiation feedback and all physical terms, i.e., mass, energy, and momentum, in the mechanical feedback. On the other hand, Model 6 (E0) adopts a treatment similar to that in SDMH05 as it assumes the same mechanical feedback efficiency, only includes the mechanical energy feedback and distributes it into the bottom layer of the grid, neglecting the mass and momentum added back into the flow.

Models 1-6 adopt the standard (high) efficiency $\epsilon_{\rm w} = 5\times10^{-3}$, as SDMH05 and JNB09 and Models 7-12 assume a factor of 20 lower efficiency, perhaps in better accord with observationally based estimates (Moe et al. 2009; Arav et al. 2010) and Models 13-18 adopt other efficiencies to show how final properties depend on the assumed mechanical efficiency.

3.1. *High efficiency models*

To mimic the common treatment (e.g., SDMH05, JNB09), we build the Model 6 (E0) that only includes the Mechanical energy feedback with the standard (high) efficiency $\epsilon_{\rm w} = 5\times10^{-3}$. In this model, we estimate the mass inflowing to the SMBH, convert it to energy with the given efficiency, and add this energy only into the bottom layers of the surrounding gases. For comparison, Model EPM0-R has identical efficiency but adds also mass and momentum to the bottom layers using Equations (5a-d) with $\eta = 9$, as appropriate for the chosen efficiency and wind velocity of $v_{\rm w,10} = 1$. These two models are shown as blue and green lines in Figure 1. We see that allowing for momentum and mass feedback reduces the black hole growth by a factor of 1000. The more consistent model has a much lower final X-ray luminosity and final SMBH Eddington ratio. The effect of including or not including radiative heating is relatively minor, as can be seen by comparing Models 3 and 4 or 1 and 2. Also the mechanical energy feedback is considerably less important (as expected) than the momentum input, as can be seen by comparing Models 4, 5, and 6. Finally it might be thought that some of the effects observed in these comparisons are due to the change from Paper I of adding the feedback to the bottom layers alone in the present simulations, rather than over a distributed range of radii to mimic the effects of due to a broad line wind. But comparison between Models 1 and 3, where

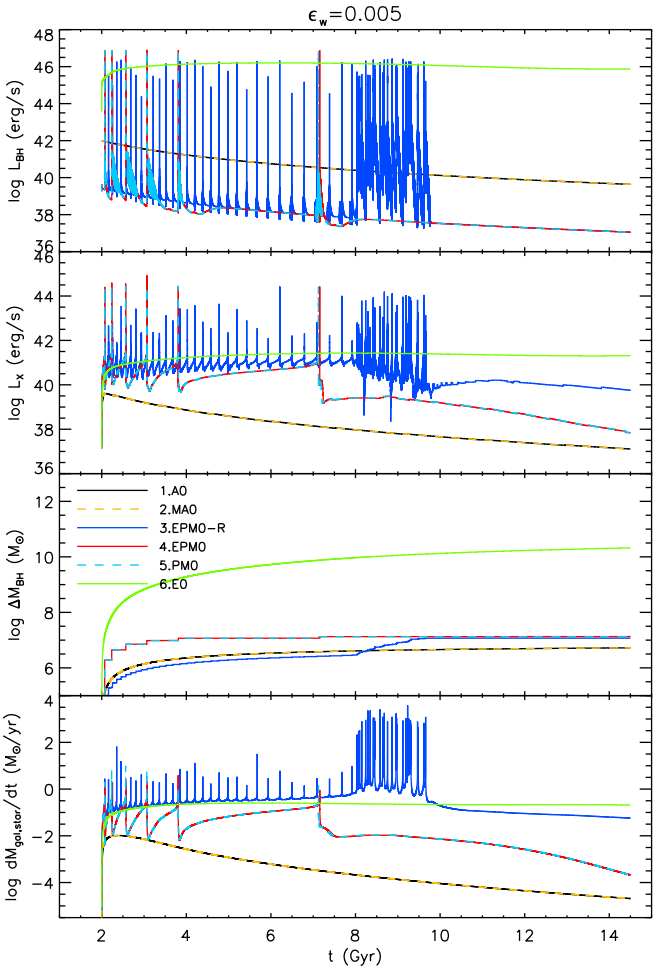

FIG. 1.— Models 1-6 with constant and high mechanical efficiency $\epsilon_{\rm w} = 5\times10^{-3}$ ($\eta = 9$). From top to bottom, the SMBH luminosity, X-ray luminosity, mass accreted on the central SMBH, and star formation rate are shown with different line types and colors as indicated in the third panel. Note how the model that excludes momentum feedback, "E0", has by far the highest growth of the central SMBH.

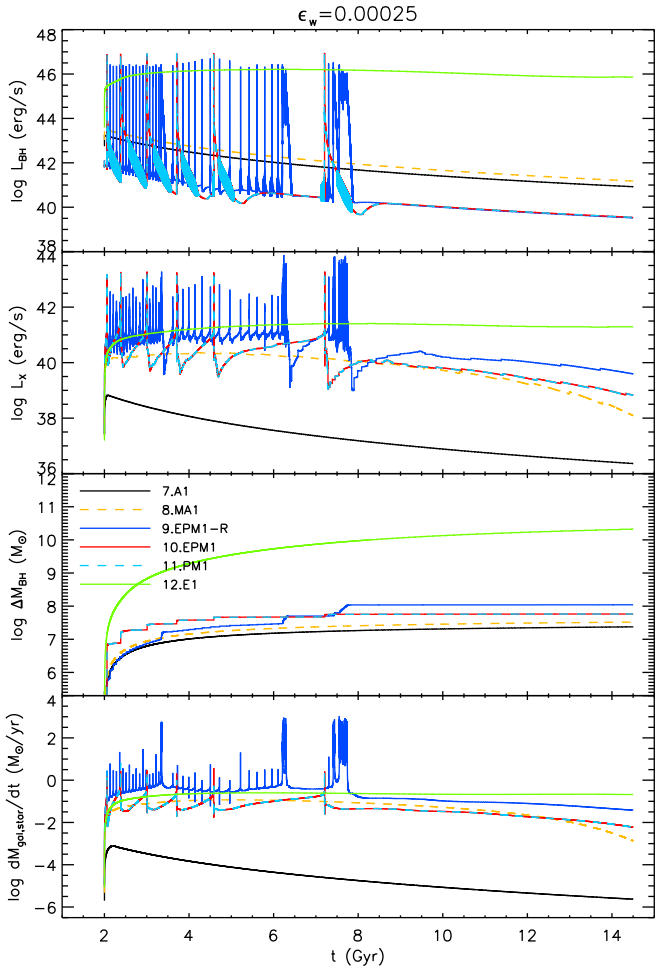

FIG. 2.— Models with constant and low (observation based) mechanical efficiency, $\epsilon_{\rm w} = 2.5\times10^{-4}$ ($\eta = 0.45$). From top to bottom, the SMBH luminosity, X-ray luminosity, mass accreted on the central SMBH, and star formation rate are shown, colors and line types as in Figure 1. Again momentum feedback is the most important physical process in protecting the central SMBH from excessive growth.

there are only small differences (and Model 1 is identical to A0 of Paper III), shows that the differences which may be attributed to distributed feedback are small. In summary, examination of Models 1-6 shows that including momentum drastically increases the effects of feedback.

3.2. *Low efficiency models*

Next, we turn our attention to Models 7-12 which have a much lower mechanical efficiency than typically assumed and it is at a level better in accord with existing (and highly imperfect) observational indications. The value for the dimensionless parameter η in these cases is only 0.45 (i.e. of order unity), so that we expect that inclusion or exclusion of the mass and momentum input will make relatively less difference. What do we find? In fact, the differences are reduced by about half an order of magnitude (0.5 dex), but it remains true that the Model 12 (like Model 6), without either momentum feedback or radiation, has an unacceptably large growth of the central SMBH and an unacceptably large final SMBH luminosity, as shown in Figure 2. Models 6 and 12 also show thermal X-ray emission greater than 10^{41} erg/s, which is on the upper side of what is typically observed in normal elliptical galaxies.

We summarize the properties of Models 1-12 in Figure 3 showing the present-day (14 Gyr) SMBH mass in solar mass versus X-ray gas and optical stellar luminosities. We show the high efficiency models (Models 1-6) in blue and the low efficiency models (Models 6-12) in red. The fiducial models, Models EPM0-R and EPM1-R with mass and momentum feedback, and Models E0 and E1 that only include energy feedback, are marked with their model numbers. As discussed above, including the momentum and mass feedback not only significantly reduces the SMBH growth but also results in a much lower final X-ray luminosity and final SMBH Eddington ratio.

3.3. *Wind efficiency dependence of bottom-layer models*

We test eight different values of $\epsilon_{\rm w}$ for models ranging from 5×10^{-6} to 5×10^{-3} for models with the bottom-layer treatment and all feedback physics activated (i.e. Models EPM#-R). These models correspond to Models 3, 9, and 13-18 in Table 1. We summarize the results at the epoch of 14 Gyr in Figure 4, where the least square linear fits of several global quantities of interest are also given. Note here that the growth of SMBH mass and

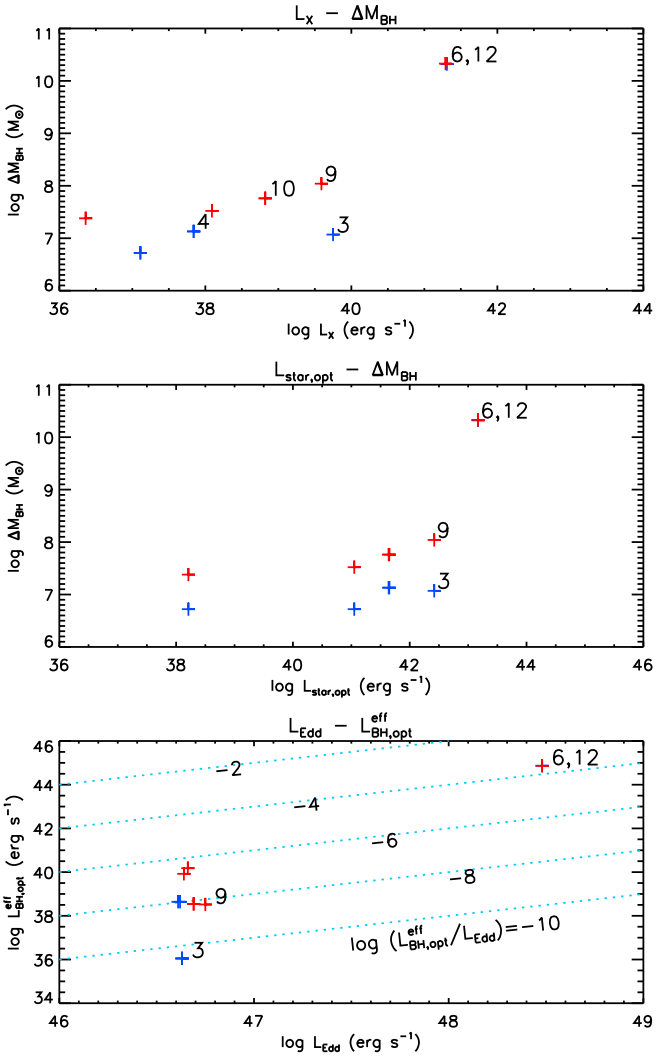

FIG. 3.— Distribution of all models in the mass-luminosity diagram measured at z=0, where different colors show different wind efficiencies and η values ($\epsilon_{\rm w} = 5\times10^{-3}$ and $\eta = 9$ for blue, $\epsilon_{\rm w} = 2.5\times10^{-4}$ and $\eta = 0.45$ for red). The distribution of models in the Eddington luminosity - effective SMBH luminosity plane is shown in the bottom panel. Five diagonal lines (from top to bottom) show $l_{\rm BH}^{\rm eff} = L_{\rm BH,opt}^{\rm eff}/L_{\rm Edd}$= 10^{-2}, 10^{-4}, 10^{-6}, 10^{-8}, 10^{-10} respectively.

the BH luminosity Eddington ratio are decreasing functions of $\epsilon_{\rm w}$. If the feedback efficiency is low, too much mass is accreted to the central SMBH, as expected. In the case of the gas mass and the predicted X-ray luminosity of the hot ISM, they are decreasing functions with increasing wind efficiency but with large scatters. We also show the total mechanical feedback energy (i.e. $\Delta E_{\rm w} = \epsilon_{\rm w}\Delta M_{\rm BH}c^2$) in the last panel, which increases as the wind efficiency increases. In this case as in several of the others, while the behavior is approximately monotonic in the direction expected, the approximate power law index is much less than unity, since larger efficiency gives a larger value for our dimensionless parameter, η, and thus a smaller fraction of the inflowing gas is actually accreted onto the central SMBH.

3.4. *The effect of mass removal from the circumnuclear disk on purely radiative models*

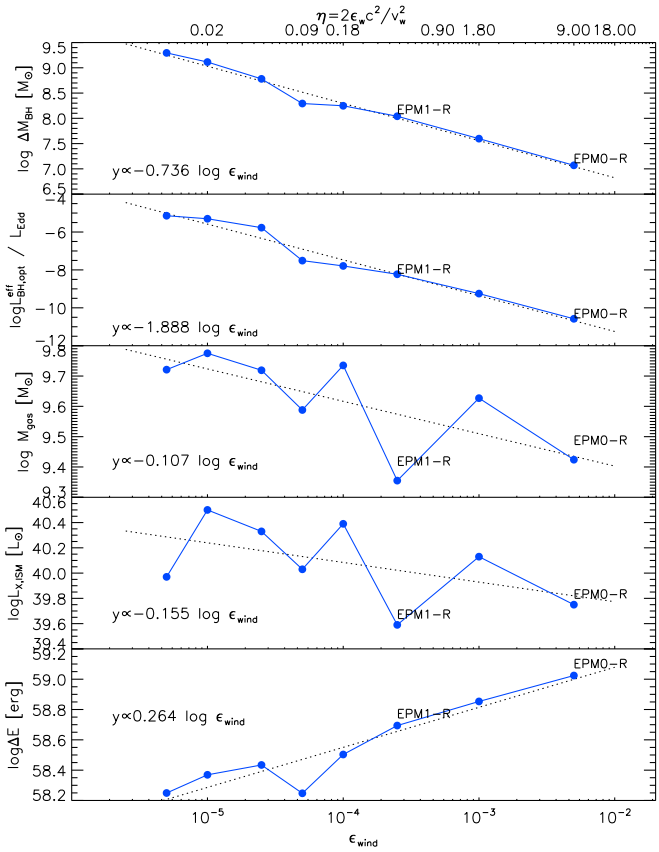

FIG. 4.— Dependencies of present-day, global quantities of EPM#-R models in Table 1, as a function of mechanical efficiency $\epsilon_{\rm w}$. From top to bottom, the SMBH mass growth, BH Eddington ratio, galaxy gas mass inside 10 $R_{\rm e}$, X-raygas luminosity, and total wind feedback energy are shown. The linear fits to the data are shown in dotted lines, and the fitting results are shown in each panel. As expected, the assumption of a higher wind energy efficiency does correspond to greater feedback effects, but at a much less than linear rate.

In line with the present exploratory discussion, it is of some interest also to check the effects of different amounts of mass removal from the circumnuclear disk via disk wind, in the case of purely radiative models. In fact, we recall that in the purely radiative models presented in Paper I (such as model RB0 in Table 2 therein) we do not add mechanical feedback to the equations of hydrodynamics, but the mass, momentum and energy fluxes of the nuclear wind (and of the jet) are nonetheless computed, in order to satisfy Equations 1–5 for assigned mechanical efficiency and fiducial nuclear wind velocity.

Therefore, purely radiative models depend indirectly on the assumed mechanical efficiency, with high-efficiency models ejecting a larger fraction of the gas from the circumnuclear wind, and therefore reducing the amount of gas available for accretion on the SMBH. Here we compare the evolution of the purely radiative model RB0 in Paper I (a model with radiative efficiency 0.1 and with high constant mechanical efficiency 5×10^{-3}), with an identical purely radiative model, in which the mechanical efficiency has been reduced to zero, therefore excluding mass loss from the circumnuclear disk.

The situation is illustrated in Figure 5, where the left panels refer to model RB0, and the right panels to the model without mass ejection from the nuclear disk. In the top panels we show the time evolution of the total

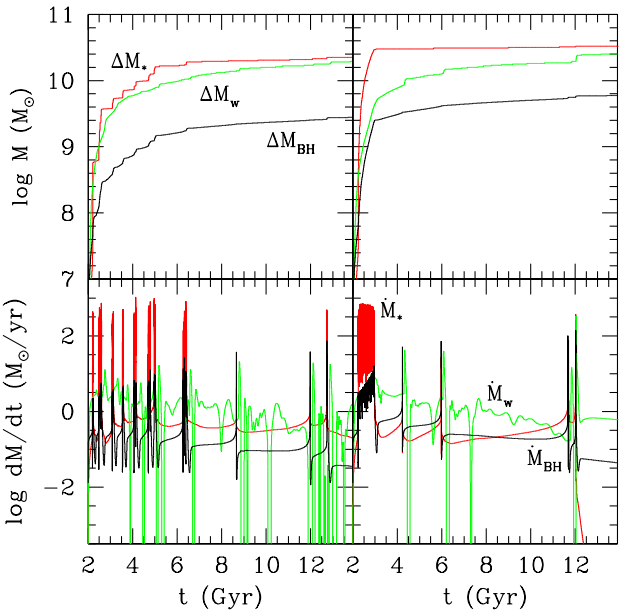

FIG. 5.— Time evolution of relevant mass budgets (top panels) and corresponding mass rates (bottom panels) in two purely radiative models (without mechanical feedback), differeing in the treatment of the circumnuclear disk mass budget. The model on the left panels is Model RB0 (see Table 2 in Paper I), while the model in the right panels is identical in all its properties to RB0, except that no mass is lost by the circumnuclear disk. Top panels: total mass accreted by the central SMBH (black), of the total mass of ISM ejected at 10 R_e (green), and of the total mass in new stars accumulated within 10 R_e (red). Bottom panels: the corresponding mass rates are identified by same colors as in top panels. The gas production of the passively evolving stellar population steadely declines from $\approx 10 M_\odot$/yr at the beginning down to less than $1 M_\odot$ at the end.

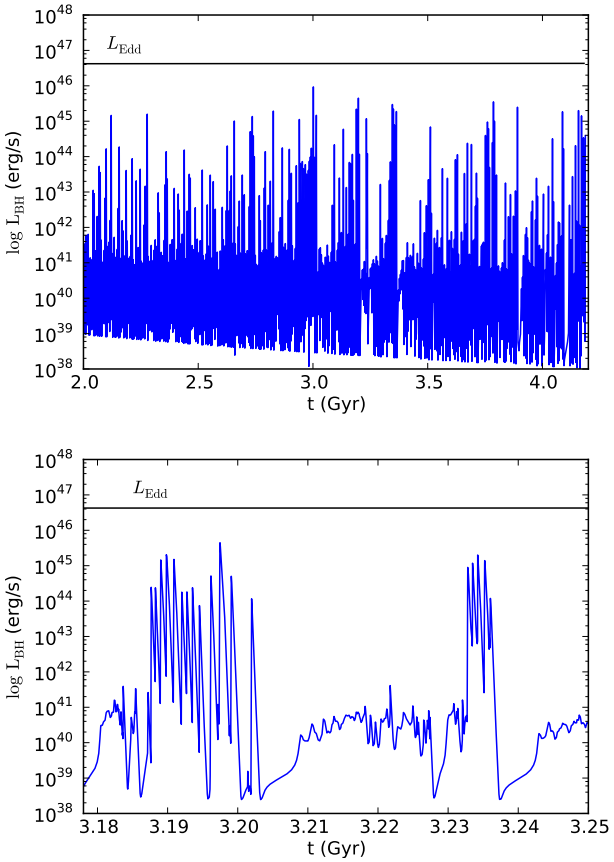

FIG. 6.— Luminosity versus time for an axisymmetric A model with $\epsilon_M = 2.5 \times 10^{-4}$. Above, the AGN luminosity for half a Gyr. Below, the AGN luminosity plotted for a shorter time showing the highly variable nature of the accretion events in two dimensions. The BH accretion is much more stochastic than the one-dimensional case, but the distribution of Eddington ratios is quite similar.

mass accreted by the central SMBH (black line), of the total ISM mass ejected by the galaxy as a galactic wind (green line), and finally of the accumulated mass in new stars (red line). In the bottom line, the corresponding rates are shown and identified with the same colors.

Unsurprisingly, the SMBH grows significantly more (by a factor of ~ 2) in the model RB0 without nuclear wind mass loss ($\log \Delta M_{\rm BH}/M_\odot \simeq 9.78$) than in the model with mass ejection ($\log \Delta M_{\rm BH}/M_\odot \simeq 9.45$). The major difference in the accretion history of the two models is particularly evident in the first Gyr of evolution, when large amounts of gas flow on the central region of the galaxy. Note how the SMBH mass of the model without nuclear mass ejection (right panels) reaches a value similar to the SMBH mass of model RB0 (left panels) at the end of the simulation. As a consequence, the gas near the SMBH is gravitationally more bound in the first model - especially at early times when the mass losses are significant. As can be seen, the star formation history in the two models is almost parallel to their SMBH accretion, and the larger radiative energy output in the model without nuclear mass ejection is accompanied by a larger starburst at early times, with a final mass of new stars of $\log \Delta M_*/M_\odot \simeq 10.5$ (red lined), to be compared with $\log \Delta M_*/M_\odot \simeq 10.36$ in RB0 model without disk mass ejection. Finally, consistently with the larger energy input of the model shown in the right panels, the galactic wind expelled a total ISM mass of $\log \Delta M_{\rm w}/M_\odot \simeq 10.4$ in the model without the disk wind, to be compared to $\log \Delta M_{\rm w}/M_\odot \simeq 10.3$ in RB0 model.

Again, this very simple experiment shows how different treatments in the mass balance equations used to describe SMBH can leads to significantly different evolutionary histories (cf. also Soker & Pizzolato 2005).

4. TWO-DIMENSIONAL MODEL COMPARISON

One dimensional models continue to be very useful in establishing the basic physical processes that are relevant for AGN feedback in giant elliptical galaxies. However, one dimensional models are not able to capture important properties of the actual systems, including the convective, Rayleigh-Taylor, and Kelvin-Helmholtz instabilities. One dimensional models must also rely on a parameterization of the global deposition of mass, energy, and momentum via the disk wind, while higher dimensional models are able to simulate the evolution of the wind self-consistently. We discuss below two-dimensional models where we have taken exactly the same galaxy model and feedback characteristics to allow comparisons that are easy to understand.

There have been many numerical simulations of BH accretion and the subsequent effects on the galaxies containing resulting AGN. However, efforts to date divide into three categories. Di Matteo, Springel & Hernquist (2005), DeBuhr et al. (2009), and Johansson, Naab & Burkert (2009) are

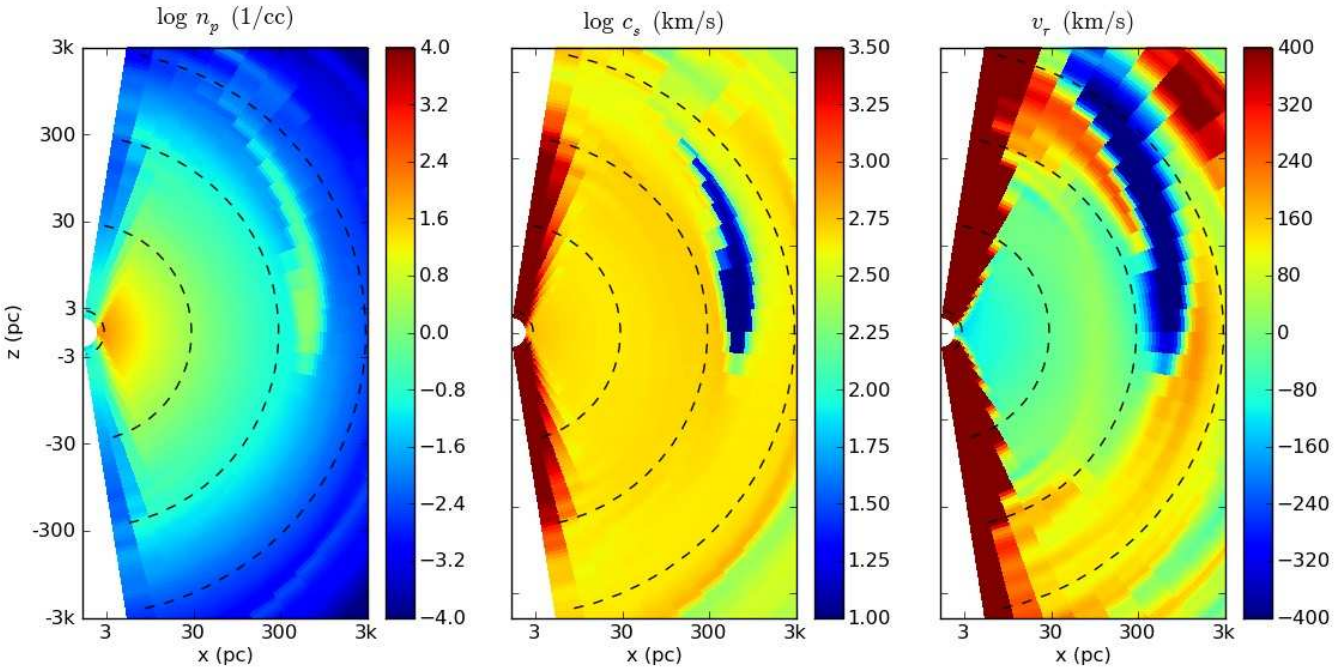

FIG. 7.— A snapshot from an axisymmetric simulation showing a cold blob falling to the center of the galaxy. On the left, log gas density in number of protons per cubic centimeter. In the center, log sound speed in kilometers per second. On the right, the radial velocity in kilometers per second. The x and y axes are logarithmic in the distance to the SMBH. The cold gas was produced by enhanced cooling in an overdense quasi-spherical shell with a covering fraction of about one third of the sphere. The gas quickly collapses to a ring with a small covering fraction and/or fragments as it freely falls to the center of the simulation.

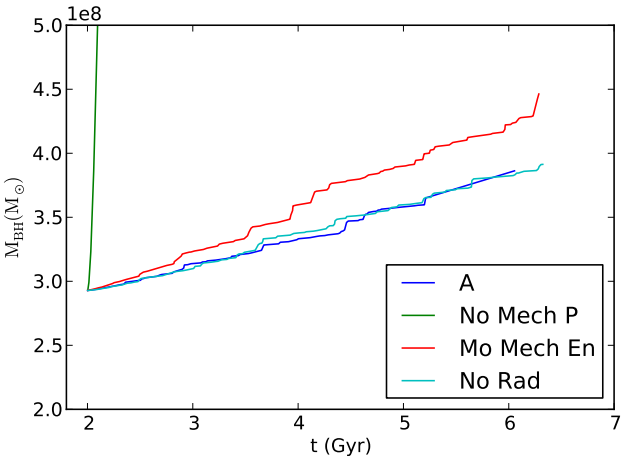

FIG. 8.— Black hole mass as a function of time for A models with $\epsilon_w = 10^{-3}$. The blue line is the fiducial case with all physics included. The green line has mechanical momentum injection turned off so that mechanical feedback is purely via energy; the SMBH grows prodigiously, indicating that mechanical momentum feedback is by far the dominant process in limiting the growth of the black hole. The red line has mechanical energy injection turned off, leaving mass and momentum injection unchanged; the SMBH grows somewhat more than the fiducial case, indicating that energy feedback plays some role in limiting SMBH growth, albeit a subdominant one. The cyan line has ϵ_{EM} set to zero so that there is no energy or momentum feedback due to radiation from the central SMBH; this is indistinguishable from the fiducial case, indicating that radiative feedback plays essentially no role in limiting SMBH growth.

examples where the simulations cover length scales from $\simeq$ 100 pc to tens of kpc and timescales from a fraction of a Myr to several Gyr. Galactic length and timescales are resolved, but the BH accretion and feedback processes are considered to be sub-resolution. Kurosawa & Proga (2009a,b) are examples of multi-dimensional simulations that cover the length scales from a few AU to $\simeq$ 1 pc. Length and timescales relevant to BH accretion are resolved, but these simulations do not approach approach galactic length or timescales, and infall rates are taken as given. Finally, Hopkins et al. (2009) and Levine et al. (2008) are examples of a multi-resolution studies of BH accretion involving progressively higher spatial resolution simulations run for progressively shorted times. The highest spatial resolution simulations go down to a fraction of a pc, run for about one mega year of simulation time. These simulations spatially resolve the accretion process, but do not reach galactic timescales. Therefore they cannot self-consistently calculate the effect of AGN feedback on the gas in the galaxy as a whole and subsequent BH accretion.

The present work is the only attempt of which we are aware to simultaneously resolve the inner length scales relevant to BH accretion (a few pc), outer length scales relevant to galaxies (tens of kpc), inner timescales relevant to BH accretion (a few years), and outer timescales relevant to galaxies and stellar evolution (10 Gyr). However, the region inside of 1 pc including the disk and BH itself are still treated as sub-resolution physics.

A full description of the two-dimensional simulations and an analysis of the similarities and differences between the one- and two-dimensional models is forthcoming. Briefly, we use the Zeus hydrodynamics code (Stone & Norman 1992) in spherical coordinates with log-spaced radial bins with $\Delta r/r = 0.1$. We have extended the code to include appropriate mass, energy, and momentum source terms corresponding to stellar evolution, star formation, type 1a and type II supernova feed-

back, radiative and mechanical feedback from AGN activity. See CO07, Papers I and III, Sazonov et al. (2005) for a full description of the input physics, which are carried over in all respects except that we have omitted the radiation pressure on dust. We require the cells to have an aspect ratio of one, giving 30 angular cells. Resolution studies have shown little difference in the SMBH accretion as a function of time as long as the opening angle of the disk wind is resolved.

The major differences between the one-dimensional code and the two-dimensional code are in the way that the two codes handle angular momentum and the disk wind from the AGN.

The one-dimensional simulations did not permit the simulated gas to have nonzero angular momentum. The 2D simulations assume axisymmetry, but compute the velocity in the ϕ direction. We must assume an angular momentum profile. In the present simulations, we avoid forming a rotationally supported gas disk by choosing the radius of centrifugal support to be inside the innermost grid cell. This allows us to avoid specifying an ad-hoc prescription for angular momentum transport.

The net specific angular momentum of the stars providing gas in the simulation is assumed to be:

$$\frac{1}{v_\phi} = \frac{1}{f\sigma} + \frac{R}{j} + \frac{d}{\sigma R} \tag{9}$$

where R is the distance to the z axis. This parameterization gives solid body rotation at small radii and constant specific angular momentum at large radii. The first term prevents the rotational velocity from exceeding $f\sigma$—at intermediate radii, there may be a region with constant velocity. When gas is created in the simulation by stellar evolution, it is given this angular momentum profile. The subsequent evolution of the gas velocity on the computational grid is governed the standard fluid dynamics conservation laws.

The one-dimensional code employs a phenomenological model to determine the radius at which energy, mass and momentum from the AGN-driven disk wind are deposited in the simulation grid. This model depends on an assumed instantaneous jet opening angle. The two-dimensional code also requires an assumption about the angular dependence of the energy, mass, and momentum injected by the disk wind at the edge of the simulation grid. Once conserved quantities have entered the simulation grid, the two-dimensional code self-consistently calculates the time evolution of the material from the disk wind; a separate phenomenological model is not required.

For the A models, the opening angle of the jet is chosen so that the disk wind covers π steradians, giving a linear opening half-angle of $\cos^{-1}\frac{3}{4} \simeq 41^\circ$. The opening angle does not depend on the BH luminosity in the A models. The 1D models simply require the jet opening angle as a parameter, but the 2D models require that the flux of material be fully specified as a function of angle from the z axis. We use

$$\frac{dq}{d\Omega\, dt} \propto \cos^2(\theta) \tag{10}$$

where q is mass, energy, or radial momentum, Ω is solid angle, and θ is the angle from the z axis. This parameterization gives half of input material within a half opening angle of $\simeq 41^\circ$.

For the present purpose, the primary result from the two-dimensional models is that the qualitative conclusions already drawn from one-dimensional models remain valid. The dominant physical mechanism regulating black hole growth is momentum injected by the broad-line wind. The energy provided by the mechanical wind has a noticeable but comparatively small effect. The effect of other feedback mechanisms is much smaller than either the mechanical momentum or mechanical energy.

Figure 6 shows the AGN luminosity versus time for one of the two-dimensional models with a mechanical efficiency of $\epsilon_{\rm w} = 0.001$ (corresponding to the one-dimensional model EPM2-R). The primary difference in the SMBH growth between the one- and two-dimensional models is that the two-dimensional models have much more stochastic growth. There quiescent periods are not as quiescent, and the spacing between the major bursts is not as regular in time. Both of these are due to instabilities present in multiple dimensions: quasi-spherical shells of cold gas are able to fragment and fall into the center bit by bit rather than as a single large shell. In the one-dimensional simulations, bursts of accretion form a hot central bubble that is able to prevent further accretion until the hot bubble cools—this often leads to very regular spacing of accretion events in time.

In two-dimensional simulations, a similar hot bubble is formed, but cold gas is able to reach the center via Rayleigh-Taylor and convective instabilities. An example of this is shown in Figure 7. Hot gas simply moves out of the way leading to much more stochastic SMBH accretion with bursts much more closely spaced in time.

Figure 8 shows the SMBH mass versus time for several two-dimensional simulations where each physical process is turned off in turn, allowing us to identify which ones are negligible and which ones play a dominant role in regulating SMBH growth. Without mechanical momentum injection, the SMBH grows in a fashion only limited by $L_{\rm Edd}$. Without mechanical energy injection, the SMBH grows about a factor of two faster than the fiducial case. Mechanical energy plays a role, but it is much less important than mechanical momentum input.

Turning off *all* radiative feedback processes by setting $\epsilon_{\rm EM} = 0$ has little effect on the SMBH growth. Making this choice eliminates gas heating as computed by the expressions in Sazonov et al. (2005), momentum provided by the absorption of those same photons, as well as momentum provided by electron scattering that determines the Eddington limit. The code does not impose the Eddington limit—it allows the accretion to be limited self-consistently by adding the Eddington force to the momentum equation. Therefore setting $\epsilon_{\rm EM} = 0$ means that the SMBH would not be limited by radiative momentum. In spite of this, the mechanical feedback is able to keep the accretion rate to physically plausible values. The actual optical depth in our simulation for electron scattering is typically small compared to unity. This is consistent with observations which show that only a minority of AGNs are "Compton thick".

5. DISCUSSION

The primary purpose of this paper is to quantitatively show, based on one- and two-dimensional computations,

exactly which processes are most important during AGN feedback episodes; which processes are most useful in protecting the central SMBH from excessive mass growth and which have most effect on the ambient galaxy. After a central outburst, the mechanical energy must be communicated to the ambient gaseous fluid by a wind and we, in fact, see these winds in luminous galaxies labeling them "broad-line regions" with outflow velocities observed to be $\sim 10,000$ km/s covering conical regions subtending 20-25 % of the sky. These winds *must* carry mass and radial momentum to the ambient fluid, reducing thereby the mass deposited on the central SMBH and adding a driving component which cannot be reradiated away by thermal processes. Equations 5a-d summarize the physics, with the dimensionless parameter η, indicating the importance of mass and momentum outflows.

In the case of an assumed high mechanical efficiency ($\epsilon_{\rm w} = 0.005$), we find that, if we suppress the mass and momentum input, then the SMBH grows by over a factor of 100 more than if momentum and mass flux were properly included in the calculation, and reaches masses $> 10^{10} M_{\odot}$ in both one- and two-dimensional calculations. Turning on or off the energy input has relatively much less effect, altering the SMBH growth by roughly a factor of 2. Ignoring the mass and momentum feedback inputs also leaves the galaxy with a central optical luminosity from the AGN which is orders of magnitude brighter than is seen in nearby elliptical systems.

Compared to these dramatic effects, the uncertainty due to not knowing accurately the wind efficiencies has a relatively minor effect. Reducing the efficiency by a factor of 20 from 5×10^{-3} to 2.5×10^{-4} reduces the wind energy output by only a factor of 2 (to $10^{58.7}$ erg) and reducing the efficiency by another factor of 10 reduces the wind energy output by only another factor of 2.

We also found that redirecting much of the inflowing mass into a BAL wind has, by itself, an important effect on models with only radiative feedback. In those computations, which do not allow for the redirection, the central SMBH again grows far too much in both the one- and two-dimensional computations.

In summary, it eventuates that enforcing the conservation of mass, momentum and energy provides extremely useful constraints in estimating the growth of central SMBHs and the feedback effects on the surrounding galaxies.

We benefited from useful conversations with Lars Hernquist, Thorsten Naab, Eve Ostriker and Elliot Quataert. J.P.O. and E.C. acknowledge the support of NSF grant AST-0707505. G.S.N. acknowledges the support of the Princeton University Council on Science and Technology.

REFERENCES

Arav, N. et al. 2010, ApJ, submitted
Arieli, Y., Rephaeli, Y., & Norman, M. L. 2010, ApJ, 716, 918
Barnes, J. E., & Hernquist, L. E. 1991, ApJ, 370, L65
Begelman, M. C., Blandford, R. D. & Rees, M. J. 1980, Nature, 287, 307
Bell, A. R. 1978, MNRAS, 182, 147
Blandford, R. D. & Ostriker, J. P. 1978, ApJ, 221, L29
Blandford, R. D. & Eichler, D. 1987, Phys. Rep., 154, 1
Booth, C. M., & Schaye, J. 2009, MNRAS, 398, 53
Ciotti, L., D'Ecole, A., Pellegrini, S. & Renzini, A., 1991, 376, 380
Ciotti, L., & Ostriker, J. P. 2001, ApJ, 551, 131
Ciotti, L., & Ostriker, J. P. 2007, ApJ, 665, 1038 (CO07)
Ciotti, L., Ostriker, J. P., & Proga, D. 2009, ApJ, 699, 89 (Paper I)
Ciotti, L., Morganti, L., &de Zeeuw, P. T. 2009, MNRAS, 393, 491
Ciotti, L., Ostriker, J. P., & Proga, D. 2010, ApJ submitted, arXiv:astro-ph/1003.0578 (Paper III)
Dai, L., Fuerst, S. V., & Blandford, R. 2010, MNRAS, 402, 1614
DeBuhr, J., Quataert, E., Ma, C.-P., & Hopkins, P., 2009, arXiv:astro-ph/0909.2872
Di Matteo T., Springel V., & Hernquist L., 2005, Nature, 433, 604
Fabian, A. C., Vasudevan, R. V., Mushotzky, R. F., Winter, L. M., & Reynolds, C. S. 2009, MNRAS, 394, L89
Fujita, Y., Kohri, K., Yamazaki, T., & Kino, M. 2007, ApJ, 663, L61
Gaspari, M., Melioli, C., Brighenti, F., & D'Ercole, A. 2010, arXiv:astro-ph/1007.0674
Hopkins, P. F., Murray, N., & Thompson, T. A.
Jaffe, W. 1983, MNRAS, 202, 995
Jiang, Y.-F., Ciotti, L., Ostriker, J. P., & Spitkovsky, A. 2010, ApJ, 711, 125
Johansson, P. H., Naab, T. & Burkert, A. 2009, ApJ, 690, 802
King, A. R. 2003, ApJ, 596, 27
Krongold, Y. et al. 2007, ApJ, 659, 1022
Kurosawa, R., & Proga, D. 2009a, ApJ, 693, 1929
Kurosawa, R., & Proga, D. 2009b, MNRAS, 397, 1791
Kurosawa, R., Proga, D., & Nagamine, K. 2009, ApJ, 707, 823
Levine, R., Gnedin, N. Y., Hamilton, A. J. S. & Kravtsov, A. V. 2008, ApJ, 678, 164
Li, C., Kauffmann, G., Heckman, T. M., Jing, Y. P., White, S. D. M. 2008, MNRAS, 385, 1903
Magorrian, J., et al. 1998, AJ, 115, 2285
Mathews, W. G. 1983, ApJ, 272, 390
McCarthy et al. 2010, MNRAS in press, arXiv:astro-ph/0911.2641
McKinney, J. C., & Gammie, C. 2004, ApJ, 611, 977
Metzler, C. A., & Evrard, A. E. 1994, ApJ, 437, 564
Moe, M., Arav, N., Bautista, M. A., & Korista, K. T. 2009, ApJ, 706, 525
Narayan, R. & Yi, I. 1994, ApJ, 428, L13
Ostriker, J. P. 1983, ApJ, 273, 99
Padovani, P., & Matteucci, F. 1993, ApJ, 416, 26
Proga, D., Stone, J. M., & Kallman, T. R. 2000, ApJ, 543, 686
Proga, D. & Kallman, T. R. 2004, ApJ, 616, 688
Proga, D. 2007, ApJ, 661, 693
Reeves, J. N et al. 2009, ApJ, 701, 493
Sazonov, S. Y., Ostriker, J. P. & Sunyaev, R. A. 2004, MNRAS, 347, 1445
Sazonov, S. Y., Ostriker, J. P., Ciotti, L., & Sunyaev, R. A. 2005, MNRAS, 358, 168
Shin, M-S., Ostriker, J. P., & Ciotti, L. 2009, ApJ, in press, arXiv:astro-ph/0905.4294
Shull, J. M. 1983, ApJ, 264, 446
Silk, J. & Nusser, A. 2010, arXiv:astro-ph/1004.0857
Sironi, L. & Socrates, A. 2010, ApJ, 710, 891
Soker, N. & Pizzolato, R. 2005, ApJ, 622, 847
Soltan, A. 1982, MNRAS, 200, 115
Springel V., Di Matteo T., Hernquist L., 2005, MNRAS, 361, 776 (SDMH05)
Sternberg, A., & Soker, N. 2008, MNRAS, 384, 1327
Stoll, R., Mathur, S., Krongold,Y., & Nicastro, F. 2009, arXiv:astro-ph/0903.5310
Stone, J. M., & Norman, M. L. 1992, ApJS, 80, 753
Thompson, T. A., Quataert, E., & Murray, N. 2005, ApJ, 630, 167
Yu, Q., & Tremaine, S. 2002, MNRAS, 335, 965